ZnSe Nanobelts and Nanowires Synthesized by a Closed Space Vapor Transport Technique

ARTICLE *in* THE JOURNAL OF PHYSICAL CHEMISTRY C · JANUARY 2007

Impact Factor: 4.77 · DOI: 10.1021/jp067556e

ZnSe Nanobelts and Nanowires Synthesized by a Closed Space Vapor Transport Technique

Z. D. Hu,[†] X. F. Duan,[†] M. Gao,[‡] Q. Chen,[‡] and L.-M. Peng*,[‡]

Beijing National Laboratory for Condensed Matter Physics, Institute of Physics, Chinese Academy of Science, P.O. Box 603, Beijing 100080, China, and Key Laboratory for the Physics and Chemistry of Nanodevices and Department of Electronics, Peking University, Beijing 100871, China

Received: November 15, 2006; In Final Form: December 20, 2006

ZnSe nanobelts and nanowires have been simultaneously synthesized by a closed-space vapor transport technique without using any carrier gas. The products are characterized by scanning electron microscopy, transmission electron microscopy, Raman spectroscopy, and photoluminescence spectroscopy. It is shown that the nanobelts and nanowires are 50−90 nm in thickness or diameter and hundreds of micrometers in length. Structure analysis indicates that the nanowires take the zinc blende structure, while the nanobelts are single crystalline or bicrystalline wurtzite phase. The as-synthesized products exhibit rich Raman modes and a strong near-band-edge luminescence peak centered at 476 nm. The nanobelts and nanowires grow via a vapor−solid mechanism mediated by a polycrystalline ZnSe film.

1. Introduction

In recent years, there has been increasing interest to synthesize various one-dimensional (1D) semiconductor materials such as nanotubes, nanowires, and nanobelts. Their peculiar structure and size often render materials with enhanced physical and chemical properties that are useful in a variety of technological applications such as light emission,[1] field emission,[2] solar cell,[3] and catalysis.[4] ZnSe is an important direct band gap semiconductor with a wide band gap of 2.68 eV[5] and a large exciton binding energy (21 meV)[6] and a promising candidate in optoelectronic devices including laser diodes, light-emitting diodes, and photodetectors. Since the demonstration of a ZnSe-based blue-green laser in 1991,[7] great progress has been made in fabricating various ZnSe nanostructures (nanowires, nanobelts, nanorods, and nanoneedles) by employing different techniques, such as molecular-beam epitaxy (MBE),[8] laser ablation,[9] metal organic chemical vapor deposition (MOCVD),[10] and thermal evaporation.[11] Among them, thermal evaporation is a simpler and less expensive method. In a conventional thermal evaporation or chemical vapor deposition (CVD) experiment, continuous carrier gas feed, for example, H_2, Ar, N_2, or He, is required and used for conveying the source vapor to the desired zone. However, the imposed carrier gas transport may lead to component separation of the source in the deposition zone. In the extreme case, only the single-component products are obtained.[12]

In this paper, we report an improved thermal evaporation approach to the synthesis of ZnSe nanobelts and nanowires. No carrier gas is used, and the vapor transport and deposition are conducted in a closed space. At an elevated temperature, the evaporant produces a pressure difference between the source and the deposition substrate, which drives the vapor to diffuse to the low-pressure zone. A thin polycrystalline ZnSe film forms first. The nanobelts and nanowires then grow from the ridges and vertexes of the ZnSe polycrystals, respectively. The nanowire and nanobelt growth is in a stable manner and only ZnSe is obtained in the deposition zone.

2. Experimental Section

The ZnSe nanobelts and nanowires were simultaneously synthesized in a horizontal tube furnace. About 0.2 g of ZnSe powder (99.99%, Sigma Aldrich) was loaded in a quartz boat. The boat was then transferred to the center region of an alumina tube inserted in the furnace. Several cleaned Si wafers coated with ∼2 nm thin gold films were placed about 15 cm from the ZnSe source as the deposition substrates. Initially, the system was sealed and evacuated by a mechanical rotary pump to a base pressure of 5×10^{-2} Torr. The system was then backfilled with high-purity hydrogen (99.999%) to a pressure of ∼100−300 Torr. Thereafter, the furnace was sealed at both ends and heated up to 1173 K in 90 min and maintained at this temperature for 120 min. After this process, the furnace was cooled naturally down to room temperature. A bright-yellow-colored product was observed on the Si substrates.

The morphological and structural features of the as-prepared products were investigated by field emission scanning electron microscopy (FESEM, Philips XL30-S-FEG) and transmission electron microscopy (TEM, Philips CM200, at 200 kV). A Raman spectrum was recorded using a JY-T64000 spectrometry system ranging from 100 to 600 cm^{-1} at room temperature. The 532-nm line of an Ar ion laser was used for excitation, with an output power of 1.5 mW. Room-temperature photoluminescence (PL) measurements were performed using a 442 nm He−Cd laser as the excitation source.

3. Results and Discussion

Figure 1a shows the general morphology of the as-synthesized products grown on the Au-coated Si substrates. There are plenty of wirelike structures with typical length ranging from tens to hundreds of micrometers. A magnified SEM micrograph is shown in Figure 1b, revealing that long nanobelts and nanowires are the two dominant components of the products. The nanowires have diameters of 50−90 nm. The typical width of nanobelts

* To whom correspondence should be addressed. E-mail address: lmpeng@pku.edu.cn.
[†] Chinese Academy of Science.
[‡] Peking University.

10.1021/jp067556e CCC: $37.00
Published on Web 01/30/2007

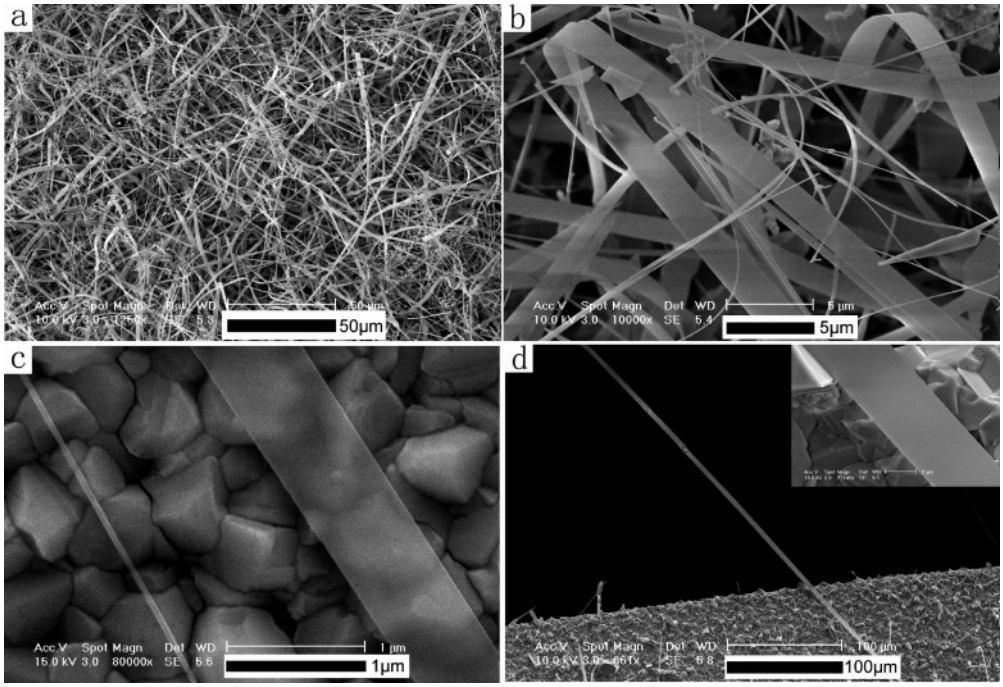

Figure 1. Representative SEM images of ZnSe nanostructures: (a) low-magnification SEM image of the as-synthesized products, (b) high-magnification SEM image, illustrating that the products consist of nanobelts and nanowires, (c) individual typical nanowire and nanobelt with a smooth and uniform shape lying above a polycrystalline film, and (d) an ultralong nanobelt growing beyond the Si wafer. The inset is a magnified image.

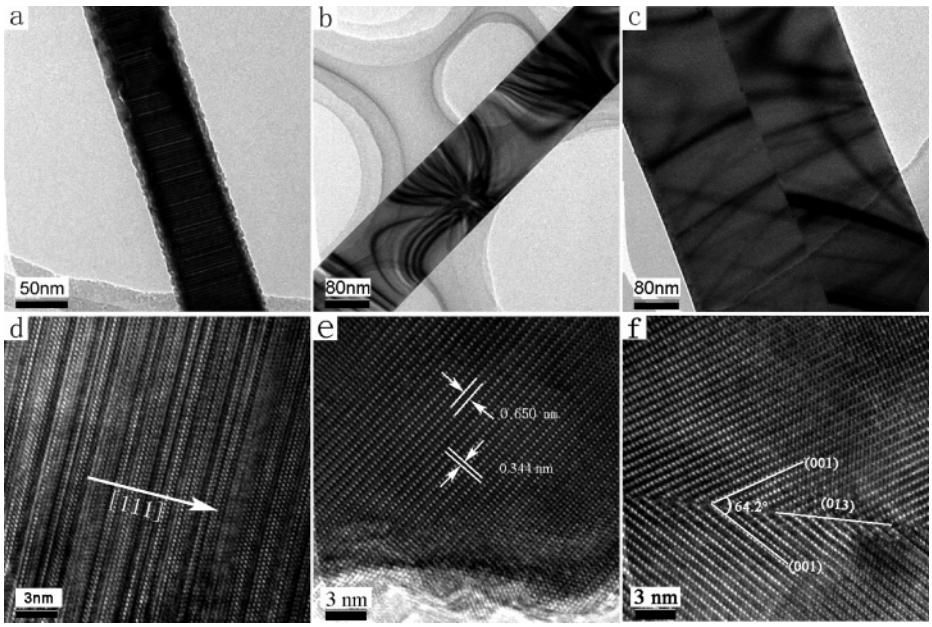

Figure 2. TEM and HRTEM micrographs of ZnSe nanowires and nanobelts: (a) TEM image of a nanowire showing obvious bright/dark contrast normal to the growth direction through the entire length, (b) TEM image of a typical nanobelt with a uniform shape, (c) TEM image of a bicrystal nanobelt displaying clear grain boundary at the center, (d) HRTEM image of the nanowire, revealing numerous stacking faults along[111] direction of cubic ZnSe, (e) HRTEM image of the single-crystal nanobelt, and (f) HRTEM image of the bicrystal nanobelt, exhibiting an atomically abrupt grain boundary of 64.2°.

varies from hundreds of nanometers to several micrometers, and their thickness and length are of the same magnitudes as those of the nanowires. Figure 1c illustrates an individual nanowire and a nanobelt which lie above the well-faceted ZnSe thin film confirmed by the following analysis. Figure 1d exhibits an ultralong nanobelt growing beyond the Si substrate, which is more than 560 μm in length and about 4 μm in width. The inset in Figure 1d is an enlarged image of the nanobelt, displaying that the nanobelt has a smooth and uniform shape. Compared with the conventional thermal evaporation approach,[11,21] the closed space vapor transport method produces ZnSe nanostructures with a narrower size distribution and a longer shape.

The structure of the products was further investigated by utilizing TEM and high-resolution TEM (HRTEM). Careful TEM observations indicate that the samples mainly include three types of microstructures: ZnSe nanowires (Figure 2a), single-crystal nanobelts (Figure 2b), and bicrystal nanobelts (Figure 2c). It is roughly estimated that the ratio of the nanowires to the nanobelts is 1:3. As shown in Figure 2a, most of the nanowires exhibit alternating bright/dark contrast perpendicular

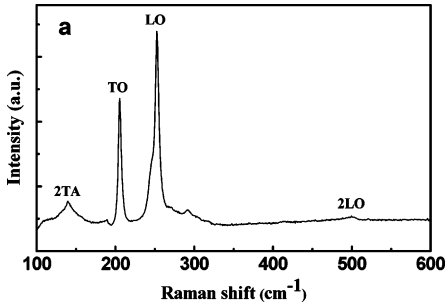

Figure 3. Room-temperature Raman spectrum of the ZnSe nanostructures.

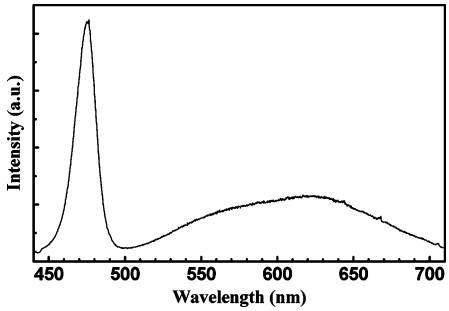

Figure 4. Room-temperature PL spectrum of the ZnSe nanostructures, showing a strong NBE emission peak centered at 476 nm and a broad and weak defect-related emission peak.

to the wires' axial direction. There is no discernible periodicity along the entire length. HRTEM analysis (Figure 2d) reveals that the nonperiodic contrast results from numerous stacking faults along cubic ZnSe[111] crystalline direction, which is the growth direction of these nanowires. Stacking faults are fairly common in II−VI and III−V semiconducting nanowires.[13−19] These planar defects always take place in the (111) facets of the zinc blende structure which are atomically identical to the polar (001) facets of the wurtzite structure. The relatively small difference in the total energy between the two phases (5.3 meV/atom for ZnSe[20]) facilitates the defect formation.

Distinguished from the nanowires, all the nanobelts take wurtzite structure evidenced by HRTEM analyses. Figure 2b exhibits a typical single-crystal nanobelt and the corresponding HRTEM image is shown in Figure 2e. The lattice spacings of 0.344 and 0.650 nm correspond to the (010) and (001) lattice planes of the hexagonal wurtzite ZnSe, respectively. Figure 2c is a typical bicrystal nanobelt showing clearly an atomically abrupt grain boundary along the central axis in the length direction. Figure 2f is the corresponding HRTEM image, revealing that the bicrystal nanobelts also take hexagonal wurtzite structure. The two (001) planes encounter at the common (013) plane, forming a symmetric tilt boundary of 64.2° at the center. Another interesting feature is noted that all the single-crystal nanobelts have a uniform shape through the entire length, whereas the bicrystal nanobelts taper from several hundreds nanometers to several tens nanometers. This interesting phenomenon deserves further exploration.

ZnSe has two stable phase structures: the cubic zinc blende at low temperature and hexagonal wurtzite at high temperature. In our case, the deposition temperature measured in a separate experiment is about 993 K. The high-deposition temperature probably results in the coexistence of the phases. This phenomenon was also observed by Li et al.[11] and Ye et al.[21] In addition, individual ZnS nanobelts and nanosaws also exhibit polytypic crystal structures,[22,23] which is because of the high deposition temperature. Lower temperature might be favorable for the formation of cubic zinc blende structure, but the optimal growth condition needs further systematic exploration.

The optical properties of the as-synthesized products were examined by Raman and PL spectroscopy. Figure 3 shows a room-temperature Raman spectrum of the as-synthesized ZnSe nanostructures. The Raman peaks at 139, 205, 252, and 504 cm^{-1} are assigned to 2TA, TO, LO, and 2LO, respectively.[24] The observation is in agreement with the results of Ye et al.[21] Figure 4 displays a representative room-temperature PL spectrum of the as-prepared products. The spectrum exhibits a strong and stable blue emission band centered at 476 nm. A weak and broad emission band ranging from 550 to 680 nm is also identified. The strong blue emission peak is usually attributed to the near-band-edge (NBE) emission of ZnSe, while the broad peak is a defect-related emission.[25] According to our SEM observations, the top layer of our sample consists of nanowires and nanobelts, which is several micrometers in its thickness. This length is much larger than the typical penetration depth[26] of 442-nm laser beam used in this work, i.e., the PL spectrum reflects mainly the properties of the near surface nanowires and nanobelts and is relatively insensitive to the substrate several microns below the surface. On the basis of the Raman and PL results, the ZnSe nanowires and nanobelts in the present study possess excellent crystallinity to display higher-order phonon modes and a strong NBE emission.

When we further inspect the samples, it is obviously seen that a blanket of polycrystalline film lies beneath the ZnSe nanowires and nanobelts. Careful study reveals that the nanobelts and nanowires always root from the ridges and vertexes of the underlying polycrystals, as demonstrated in Figure 5 and Figure 6. Meanwhile, no nanoparticles attached to the ends of the nanowires or nanobelts are found, as shown in parts a and c of Figure 6, suggesting that the vapor−liquid−solid (VLS) growth mechanism does not work in this experiment.[26] Consequently, vapor−solid process is presumed to dominate the growth.

The growth process can be divided into two main stages. First, a continuous polycrystalline ZnSe film forms on the substrates mediated by the thin Au film. At an elevated temperature, ZnSe powder evaporates and decomposes into Zn and Se vapor. The unceasing evaporation leads to a constant higher pressure than that at both blind ends. The pressure difference forces the vapor to diffuse toward the both ends and plays the same role as the carrier gas in the conventional thermal evaporation process. The deposition is based on the following reversible transport reactions

$$\mathrm{ZnSe\ (s) + H_2\ (g) \leftrightarrow Zn\ (v) + H_2Se\ (v)}$$

At a suitable temperature region, the vapor mixture undergoes a fast condensation reaction process and recombines to form single crystalline ZnSe nuclei with the help of the thin Au film. These nuclei have a high surface energy, so the interaction with the Zn or Se vapor causes continuous surface growth. Then they coagulate through particle−particle collision process, forming a continuous polycrystalline film. When the thin Au film is absent, however, only some larger ZnSe microcrystals are sparsely deposited on the plain Si substrate and no nanowires or nanobelts are obtained.

Second, nanobelts and nanowires grow from the ridges and vertexes of these polycrystals, as shown in Figures 5 and 6, respectively. The well-faceted polycrystalline films present high chemical activity at high temperature, especially at the vertexes and ridges where the forthcoming Zn and Se cluster can preferentially gather and incorporate. The continuous and stable

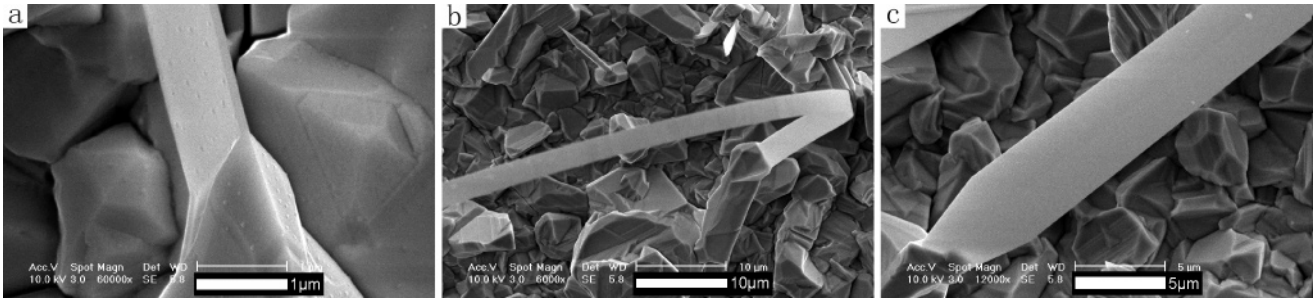

Figure 5. Representative SEM images of ZnSe nanobelts which all root from the ridges of the polycrystals.

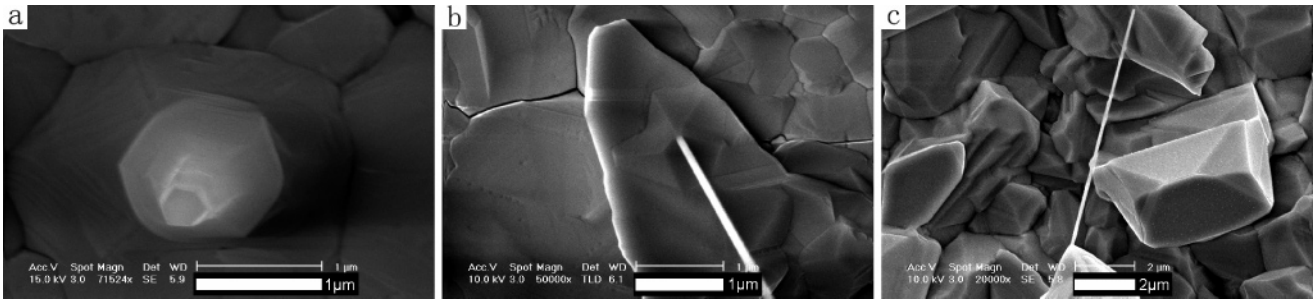

Figure 6. Typical SEM images of ZnSe nanowires, showing that they grow from the vertexes of the polycrystals. (a) Embryo nanowire with a well-faceted profile, (b) typical nanowire connected with the vertex of ZnSe polycrystals, (c) nanowire without any particle attached to the end.

feed of the source vapor results in the formation of ultralong nanowires and nanobelts. Figures 5a and 6a illustrate an initial nanobelt and nanowire with well-faceted shape, respectively. The polycrystalline ZnSe film just plays the role of seeds and facilitates the growth of the nanobelts and nanowires. The various orientations of the ZnSe polycrystals result in the polymorphic ZnSe nanostructures. H_2 in the process not only provides a reduced ambient but also promotes the vapor transport based on the above-mentioned reversible transport reaction. In the conventional process, the vapor is conveyed to deposition zone by forced diffusion, which is too fast for vapor to recombine into compound. Whereas in a closed-space vapor transport technique, the vapor generated at high-temperature zone is consumed in the deposition region and no surplus vapor is produced in the sealed space. Consequently, the established pressure gradient is stably maintained during the whole deposition process and the diffusion and deposition have no significant influence on the pressure profile. Therefore, the nanobelts and nanowires growth is in a stable manner and the component separation can be avoided. In fact, similar growth phenomenon was also observed by Zhang et al.[27] in the preparation of ZnS nanobelts.

4. Conclusion

In summary, we have fabricated ZnSe nanobelts and nanowires simultaneously by a closed-space vapor transport technique. No carrier gas is used, and the vapor transport is driven by the pressure difference between the source and the deposition zone at an elevated temperature. H_2 in the sealed system can promote the vapor diffusion. The thin Au film just facilitates the formation of the continuous polycrystalline ZnSe film, which serves to induce the growth of the nanobelts and nanowires. The products were characterized by SEM, TEM, and HRTEM. It is shown that the nanowires take cubic zinc blende structure with numerous nonperiodic stacking faults throughout the length, whereas the nanobelts possess hexagonal wurtzite structure. The nanobelts are either single crystalline phase with uniform width or tapered bicrystal structure. Their length ranges from tens to hundreds of micrometers, and their diameter or thickness is about 50−90 nm. The as-synthesized products exhibit rich Raman modes. Room-temperature PL measurement displays a strong NBE luminescence centered at 476 nm implying possible applications in nanoscale optoelectronic devices. The successful synthesis of ZnSe nanostructures employing a closed space vapor transport technique suggests that other II−VI and III−V semiconducting nanostructures might also be fabricated in a similar facile fashion. Meanwhile, the component separation is avoided.

Acknowledgment. This work is supported by the Ministry of Science and Technology (Grant No. 2006CB0N0401), National Science Foundation of China (Grant No. 10434010 and 90606026), and the National Center for Nanoscience and Technology of China.

References and Notes

(1) Huang, Y.; Duan, X. F.; Lieber, C. M. *Small* **2005**, *1*, 142.

(2) Choi, W. B.; Chung, D. S.; Kang, J. H.; Kim, H. Y.; Jin, Y. W.; Han, I. T.; Lee, Y. H.; Jung, J. E.; Lee, N. S.; Park, G. S.; Kimd, J. M. *Appl. Phys. Lett.* **1999**, *75*, 3129.

(3) Law, M.; Greene, L. E.; Johnson, J. C.; Saykally, R.; Yang, P. D. *Nat. Mater.* **2005**, *4*, 455.

(4) Kolmakov, A.; Moskovits, M. *Annu. Rev. Mater. Res.* **2004**, *34*, 151.

(5) Rujkorakarn, R.; Nelson, A. J. *J Appl. Phys.* **2000**, *87*, 8557.

(6) Zhu, Z. M.; Liu, N. Z.; Li, G. H.; Han, H. X.; Wang, Z. P.; Wang, S. Z.; He, L.; Ji, R. B.; Wu, Y. *J. Infrared Milimeter Waves* **1999**, *18*, 13.

(7) Haase, M. A.; Qiu, J.; DePuydt, J. M.; Cheng, H. *Appl. Phys. Lett.* **1991**, *59*, 1272.

(8) Cai, Y.; Chan, S. K.; Sou, I. K.; Chan, Y. F.; Su, D. S.; Wang, N. *Adv. Mater.* **2006**, *18*, 109.

(9) Jiang, Y.; Meng, X. M.; Yiu, W. C.; Liu, J.; Ding, J. X.; Lee, C. S.; Lee, S. T. *J Phys. Chem. B* **2004**, *108*, 2784.

(10) Zhang, X. T.; Liu, Z.; Li, Q.; Leung, Y.; Ip, K.; Hark, S. *Adv. Mater.* **2005**, *17*, 1405.

(11) Li, Q.; Gong, X. G.; Wang, C. R.; Wang, J.; Ip, K.; Hark, S. *Adv. Mater.* **2004**, *16*, 1436.

(12) Hu, P. A.; Liu, Y. Q.; Fu, L.; Cao, L. C.; Zhu, D. B. *Chem. Commun.* **2004**, *5*, 556.

(13) Krishnamachari, U.; Borgstrom, M.; Ohlsson, B. J.; Panev, N.; Samuelson, L.; Seifert, W.; Larsson, M. W.; Wallenberg, L. R. *Appl. Phys. Lett.* **2004**, *85*, 2077.

(14) Ahrenkiel, S. P.; Mícíc, O. I.; Miedaner, A.; Curtis, C. J.; Nedeljkovíc, J. M.; Nozik, A. *J. Nano Lett.* **2003**, *3*, 833.
(15) Li, H. W.; Chin, A. H.; Sunkara, M. K. *Adv. Mater.* **2005**, *18*, 216.
(16) Persson, A. I.; Larsson, M. W.; Stenström, S.; Ohlsson, B. J.; Samuelson, L.; Wallenberg, L. R. *Nat. Mater.* **2004**, *3*, 677.
(17) Tateno, K.; Hibino, H.; Gotoh, H.; Nakano, H. *Appl. Phys. Lett.* **2006**, *89*, 033114.
(18) Xu, X. X.; Wei, W.; Qiu, X. M.; Yu, K. H.; Yu, R. B.; Si, S. M.; Xu, G. Q.; Huang, W.; Peng, B. *Nanotechnology* **2006**, *17*, 3416.
(19) Geng, B. Y.; Liu, X. W.; Du, Q. B.; Wei, X. W.; Zhang, L. D. *Appl. Phys. Lett.* **2006**, *88*, 163104.
(20) Yeh, C. Y.; Lu, Z. W.; Froyen, S.; Zunger, A. *Phys. Rev. B* **1992**, *46*, 10086.
(21) Ye, C.; Fang, X.; Wang, Y.; Yan, P.; Zhao, J.; Zhang, L. *Appl. Phys. A* **2004**, *79*, 113.
(22) Hao, Y. F.; Meng, G. W.; Wang, Z. L.; Ye, C. H.; Zhang, L. D. *Nano Lett.* **2006**, *6*, 1650.
(23) Ding, Y.; Wang, X. D.; Wang, Z. L. *Chem. Phys. Lett.* **2004**, *398*, 32.
(24) Pages, O. M.; Renucci, A.; Brit, O.; Aulombard, R. L. *J Appl. Phys.* **1995**, *77*, 1241.
(25) Yao, T.; Takeda, T.; Watanuki, R. *Appl. Phys. Lett.* **1986**, *48*, 1615.
(26) Cui, Y.; Lauhon, L. J.; Gudiksen, M. S.; Wang, J.; Lieber, C. M. *Appl. Phys. Lett.* **2001**, *78*, 2214.
(27) Zhang, Z. X.; Wang, J. X.; Yuan, H. J.; Gao, Y.; Liu, D. F.; Song, L.; Xiang, Y. J.; Zhao, X. W.; Liu, L. F.; Luo, S. D.; Dou, X. Y.; Mou, S. C.; Zhou, W. Y.; Xie, S. S. *J Phys. Chem. B* **2005**, *109*, 18352.